Discrimination Algorithm for False Alarm Reduction in SAR Incoherent Change Detection

Alexandre B. Campos, Ricardo D. Molin Jr., Mats I. Pettersson, and Renato Machado

***Abstract*— This paper introduces an additional stage for incoherent change detection algorithms (CDAs) based on multi-layer perceptron (MLP). Pixels the CDA initially assigned as detections are re-evaluated by the MLP based on features extracted from the processed images, according to a previously performed training. The tests considered multitemporal synthetic aperture radar (SAR) images from the CARABAS-II system, in a scenario where military vehicles were concealed under vegetation. Preliminary results show that the proposed method can reduce the false alarm rate (FAR) by up to 73% for the same probability of detection.**

***Keywords*— CARABAS-II, CDA, false alarm reduction, MLP, SAR images.**

I. Introduction

Change detection is the process of identifying differences between two or more images of the same area of interest, considering polarimetric, multispectral, or multitemporal images [1]. Recognizing such changes visually may be laborious and inefficient, in such a way that this process is automatized through change detection algorithms (CDAs), which are widely used in areas such as precision agriculture [2], deforestation monitoring [3] and urban studies [4].

In the last few years, synthetic aperture radars (SAR) have become one of the main tools for monitoring the Earth's surface [1]. SAR systems can be classified as orbital or airborne, being able to generate high-resolution images due to the synthesis of a large aperture along their movement. At lower frequencies (e.g., VHF band), SAR systems have been used in applications such as ground and foliage penetration (GPR – Ground Penetrating Radar [5], FOPEN – Foliage Penetration [6]), especially for detection of covered or camouflaged structures that are not revealed by optical sensors.

In this context, the airborne SAR system CARABAS-II has been developed by the Swedish Defence Research Agency (FOI) as a tool for monitoring forested areas with FOPEN applications, operating at the lower limit of the VHF band (20-90 MHz). Change detection in forested areas is usually associated with a large number of scatters and involves a series of challenges, in such a way that FOI has published a set of 24 SAR images from a test field in northern Sweden, where 25 military vehicles were concealed under vegetation, in order to encourage the development of new CDAs [7]. The main challenge in this scenario is to sufficiently suppress the clutter[1] to achieve a false alarm rate (FAR) low enough to provide useful information to the operator of the system.

Typically, a CDA is composed of three main parts: (1) the change image processing highlights the differences between a surveillance image and one or more reference images; (2) a decision process aims to classify the pixels, or groups of these, into targets or background; (3) finally, morphological operations are employed to reduce the number of false alarms based on the resolution and other physical characteristics of the system.

In this paper, we introduce a second processing stage based on a multi-layer perceptron (MLP) after the CDA is applied. The detected pixels are tested again by the MLP, which considers features of change regions from the surveillance and reference images to discriminate targets from potential false detections. Preliminary results show that the proposed model can efficiently reduce the number of false alarms, while keeping a high probability of detection.

The remainder of this paper is organized as follows. Section II describes the considered dataset of 24 SAR images. Section III introduces the proposed model, the change detection algorithm and the training of the MLP network. In Section IV, the results are presented and discussed. Finally, Section V presents some final considerations and remarks.

II. Data Description

The change detection problem considered in this paper is based on a set of 24 SAR images acquired in 2002 with the CARABAS-II system in a boreal forest region in northern Sweden. The CARABAS-II system transmits horizontally polarized waves in a frequency range of 20-90 MHz, which ensures that the sensor only receives strong responses from objects of the order of 1 m or larger, in a way that most changes that occur in the environment, such as falling leaves and branches, are not registered in the images [6].

The imaged area has 6 km^2 (3 km $\times$ 2 km), and each pixel corresponds to an area of 1 $\times$ 1 m, which means that the considered images are analyzed as matrices with dimensions 3000 $\times$ 2000. Moreover, 25 military vehicles were deployed in regions where the forest is denser. The vehicles consist of three different models: ten TGB11, with dimensions $4.4 \times 1.9 \times 2.2$ m, eight TGB30, with $6.8 \times 2.5 \times 3.0$ m and seven TGB40, with dimensions $7.8 \times 2.5 \times 3.0$ m. Figure 1 shows an

Alexandre B. Campos, Ricardo D. Molin Jr., and Renato Machado, Graduate Program of Electronics and Computer Engineering, Aeronautics Institute of Technology (ITA), 12228-900, São José dos Campos - SP, Brazil. E-mails: beckercampos@ieee.org, rsddj@ieee.org, renatomachado@ieee.org. Mats I. Pettersson, Department of Mathematics and Natural Sciences, Blekinge Institute of Technology (BTH), 371 79, Karlskrona, Sweden. E-mail: mats.pettersson@bth.se. This study was financed in part by the Coordination for the Improvement of Higher Education Personnel (CAPES) - Finance Code 001.

[1] Unwanted signals or echoes that hinder the detection of targets.

example of one of these images, in which the 25 targets are highlighted inside the red square. Other structures like power lines, fences, rocks and constructions can also be seen as bright structures, which motivates the use of a reference image for clutter suppression.

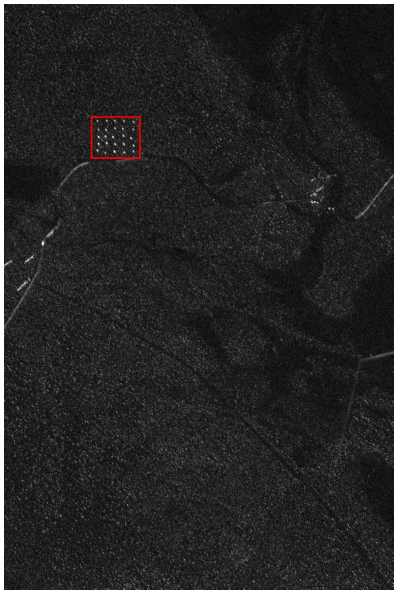

Fig. 1. Example of a SAR image from the CARABAS-II database. The targets are highlighted inside the red square.

Moreover, the 24 SAR images considered in this paper can be divided into four missions: Sigismund, Karl, Fredrik, and Adolf-Fredrik. Each mission is associated with a different target deployment, illustrated in Figure 2, and contains six images: two acquired with a flight heading of 225º, two with 135º and two with 230º. While deployments Sigismund and Karl are displayed in the top-left corner of the images with target headings of 225º and 315º, respectively, deployments Fredrik and Adolf-Fredrik are found in the bottom-right corner of the images with target headings of 225º and 270º, respectively. The headings are defined as 0º pointing towards the north and increase clockwise.

The change detection is then performed considering pairs of images from different deployments, i.e., missions. In this paper, the same 24 pairs of surveillance and reference images presented in [7] are considered for comparison purposes.

III. Proposed Model

A block diagram for the proposed model is presented in Figure 3 and can be divided into three main steps: (1) the image processing is performed by a CDA which, after an internal decision step, binarily indicates objects (groups of connected pixels) where significant changes occur between a surveillance image and a reference one; (2) a 9×9 window centered in the centroid of each detected object is considered a region of interest (ROI), where the features extraction is performed; (3) a previously trained MLP network is used to discriminate detections into a target or non-target class.

The model characteristic implies that the probability of detection is limited by the CDA, as the MLP network can only discriminate detections that are previously assigned by the CDA. Thus, the MLP block introduction aims to improve the performance of radar change detection algorithms by reducing the presence of false detections (false alarms). In this paper, a CDA based on control charts (detailed in Subsection III-A) is applied to demonstrate the proposed method, while the features and methodologies for training the MLP are shown in Subsection III-B.

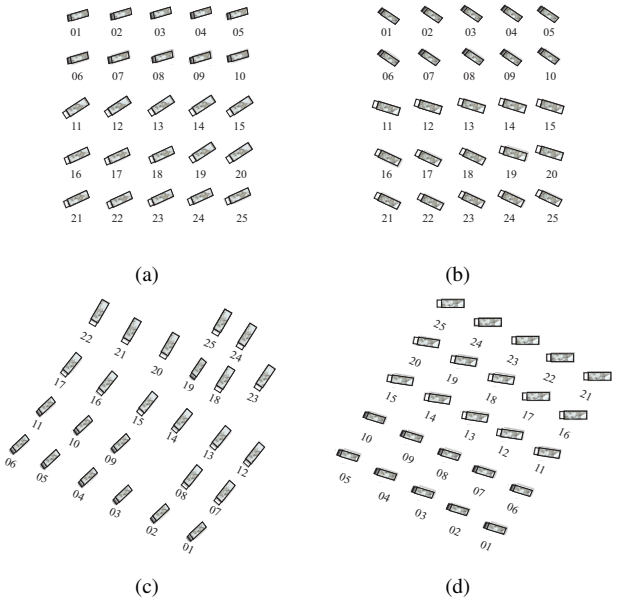

Fig. 2. Four possible missions and their respective target deployments in CARABAS-II data: (a) Sigismund, (b) Karl, (c) Fredrik and (d) Adolf-Fredrik. Details about the distribution of the 25 targets in respect to their three possible classes (TGB11, TGB30 and TGB40) can be found in [7].

Fig. 3. Block diagram of the proposed model. Two georeferenced images (z_r and z_s) are applied into a change detection algorithm (CDA), which highlights objects of interest. Each object's location and surroundings are extracted (ROI extraction), with a set of features for each object being acquired. A previously trained neural network (MLP) can then discriminate the CDA's detections as being targets or non-targets. A final georeferenced image (z_f) is then generated, where only the objects classified by the MLP as targets are maintained and thus a false alarm reduction occurs.

A. Change Detection Algorithm (CDA)

The incoherent CDA considered in this paper is adapted from [9]. This algorithm is based on a control chart technique [10] that iteratively detects outliers and thus can help to define optimal thresholds for each pair of images.

The first part of this CDA consists in generating a change image through a differencing technique, i.e., a reference image z_r is subtracted pixel by pixel from a surveillance image z_s. The resulting matrix is then normalized, i.e., subtracted by its mean and divided by its standard deviation, and a threshold is used to establish an upper control limit (UCL) and a lower

control limit (LCL). Pixels that lay outside this interval are classified as targets and the remaining ones are renormalized. This process is repeated until every pixel is found between the lower and upper limits, as can be seen in Figure 4. The output of this part is a binary image, where '1' denotes positive changes (the targets of interest, pixels above the upper limit) and '0' represents the background and negative changes.

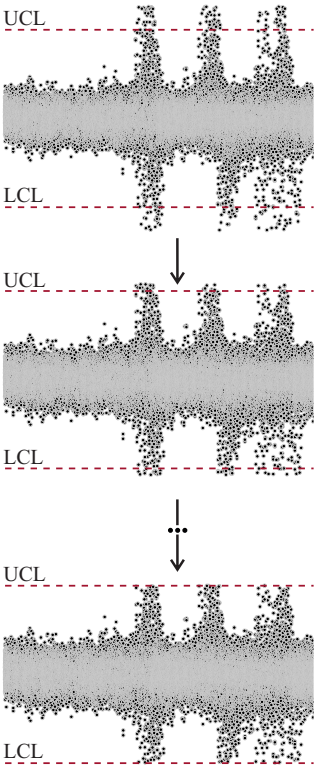

Fig. 4. Iterative process of the CDA. Pixels greater than the thresholds are considered to be part of targets (first chart) and the remaining ones are renormalized. This process is repeated until every pixel is found within the lower and upper limits (last chart).

Finally, morphological operations are employed to reduce the occurrence of false alarms (as in [7], [11]). According to the criteria adopted in [7], [9], an erosion process removes objects (groups of connected pixels) considered too small given the system resolution, while a dilation is applied to unite groups of pixels that are too close from each other, both employed with a 3×3 structural element.

The final result of the considered CDA is a binary image, in which objects of interest are highlighted. In a conventional radar target detection problem, every object would be assigned as targets and thus the number of false alarms would tend to be high.

B. Discrimination Algorithm (MLP)

The discrimination algorithm is based on MLPs, a class of feedforward neural networks, which derives from the perceptron [12]. They are distinguished from the latter by having hidden layers between the input neurons and the network output [13], with non-linear activation. The learning process of the network is supervised through a backpropagation algorithm. Due to its characteristics, it can distinguish data that are not linearly separable. An architecture example of an MLP neural network is presented in Figure 5.

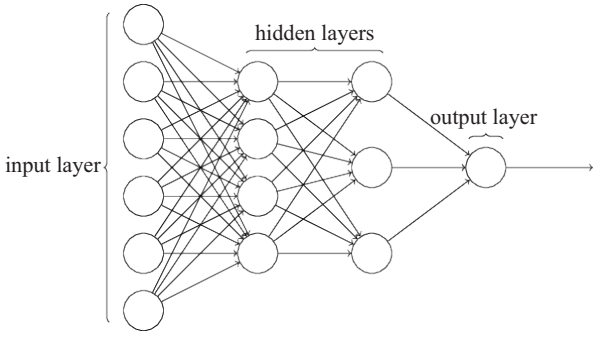

Fig. 5. Architecture for an MLP binary classification.

The choice for this class is based on the characteristics of the data (non-linearly separable) and ease of implementation. Furthermore, perceptrons and MLPs have already been applied to SAR images with different objectives: discrimination of different types of targets (vehicles) [14], [15] and noise removal [16]. Given an MLP used for binary classification, the i-th layer of the network (output neuron) can be formulated as

$$a^i = f^i(W^i a^{i-1} + b^i), \tag{1}$$

where its activation is defined in terms of the weight matrix W^i and the vector bias b^i, governed by the activation function f^i, which transforms the sum of the outputs of the previous state in an output a^i [13], defining the algorithm classification.

The weight update process is made by a backpropagation algorithm, which can be summarized as follows [17]: (1) weights initialization; (2) samples extraction from the training set; (3) propagation phase, which starts as an input vector applied in the first hidden layer and calculates the error signals between the desired answer and the obtained one; (4) backpropagation phase, which starts in the output layer and calculates the local gradients; (5) iteration between (3) and (4) with new training samples until the stopping criteria are satisfied.

The training set for the MLP consists of four image pairs that represent all four missions from the selected images (CARABAS-II). Thus, the database is compounded by 100 target samples (25 targets for each pair) and 100 background samples. For sampling the data, each of the 100 target locations is acquired, given that their positions on the field are previously known for the CARABAS-II set. The same is made for 100 pixels considered as background. For extracting the latter, two methodologies are proposed:

1) MLP I: random pixel extraction from image background;
2) MLP II: image pre-processing in order to obtain objects previously identified as false alarms (false detections) on the used CDA, aiming to extract more relevant pixels of the background.

Each sample of the training data, from a total of 200, is acquired in the following way: (1) the coordinates (x, y) from

the pixel of interest is extracted, where the pixel represents a known target, a random point in the background (MLP I) or a erroneously detected point from the CDA (MLP II); (2) a window, centered in (x, y), of size 9×9 (in a way that it can comprise the biggest target size, described in Section II) is considered for the surveillance image z_s and reference z_r; (3) features from these windows are extracted to represent the object of interest, centered in (x, y); (4) the outcome of this extraction (features vector) is used as input layer for the MLP. The extraction process is presented in Figure 6.

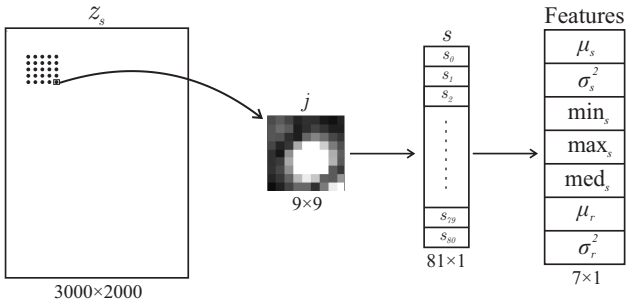

Fig. 6. Features extraction process.

In the feature vector, μ_s and μ_r represent the mean value obtained from the window for the surveillance and reference images, respectively. Analogously, the variances σ_s^2 and σ_r^2 are extracted. Furthermore, the minimum ($\min_s$), maximum ($\max_s$) and median (med_s) values of the surveillance window are also acquired. The selected features aim to represent the window with a reduced number of inputs in contrast to utilizing all the 81 pixels of the window.

Thus, for the training data 200 samples are acquired (100 target samples and 100 background samples). The MLP I approach comes from [18], but while target and randomly selected background windows can be easily distinguished, objects identified as false alarms are usually a greater challenge. Therefore, the methodology MLP II is proposed for establishing a more robust training data.

Figure 7 illustrates windows considered as target, background according to MLP I and background according to MLP II. While the first one represents a vehicle, the third one represents a fence (part of the background) with characteristics that make its rejection difficult by the majority of CDAs.

Fig. 7. Samples acquired from a surveillance image. Target, background, and a false detection mistakenly detected by the CDA, respectively.

IV. Experimental Results

Image pairs 4, 7, 13 and 22 from [7] were selected to train the algorithm. Thus, the trained algorithm was applied for the remaining 20 proposed pairs. For the CDA stage, the following thresholds were adopted: 2.75, 3.0, 3.5, 4, 4.5, 5.0 and 6.0. In order to acquire the training data samples for the MLP II methodology, 100 samples of detections mistakenly assigned as targets from the four training pairs at the threshold 2.75 were selected. Thus, after the model training, pixels previously appointed as detections by the CDA for each threshold are reassessed. "CDA + MLP I" and "CDA + MLP II" are the adopted names for the systems composed by the CDA and the two training methodologies, respectively.

The neural networks were implemented in Python, using the TensorFlow library. A batch size of 20 was used and the *rmsprop* optimizer was employed. Given the features transformations applied in this work, it was possible to reduce the computational complexity of the adopted model. Thus, for the selection of the MLP architecture, variations from one to three hidden layers were tested, besides varying the number of neurons present in each of them in quantities of 16, 32 and 64. The architectures were evaluated with respect to their precision and loss, which directly reflects the network's ability to maintain a good probability of detection while still being able to reduce the number of false alarms significantly.

The best performance was achieved using three hidden layers, each one with 16 neurons activated by a ReLU function. The output neuron is activated by a sigmoid function [17]. This architecture, for the MLP I, obtained a precision of 99% and a -25.35 dB loss. For the MLP II, the precision was 96.89% and a -9.37 dB loss.

In order to evaluate the use of this algorithm in radar change detection problems, we employ metrics such as probability of detection and false alarm rate (FAR). The first expresses the number of true detections over the total number of known targets, while the second is defined as the number of false detections per km^2. Receiver operating characteristics (ROC) curves are used to visualize the performance of an algorithm for a set of thresholds, linking the two previously cited variables. In general, we may conclude that better decision or detection performance is indicated by an ROC curve that is higher and to the left in the ROC space [19].

Figure 8 presents the comparison between the original ROC curve for the CDA (continuous blue line) and the two proposed approaches. The FAR is disposed in a logarithmic form for better visualization. The probability of detection (P_d) is limited by the CDA, and thus the MLP discriminator acts as a false alarm reducer. This is noticeable from the displacement between the original CDA curve and the proposed approaches, especially the MLP II one. Additionally, the results are disposed in Table I, which compares the FAR for each approach given a fixed probability of detection.

TABLE I

False alarm rate by probability of detection for the original CDA and with the addition of MLP I and MLP II discriminators.

P_d	FAR		
	CDA	CDA + MLP I	CDA + MLP II
0.97	0.4583	0.3792	0.1229
0.96	0.2500	0.2333	0.0917
0.95	0.2333	0.2167	0.0907

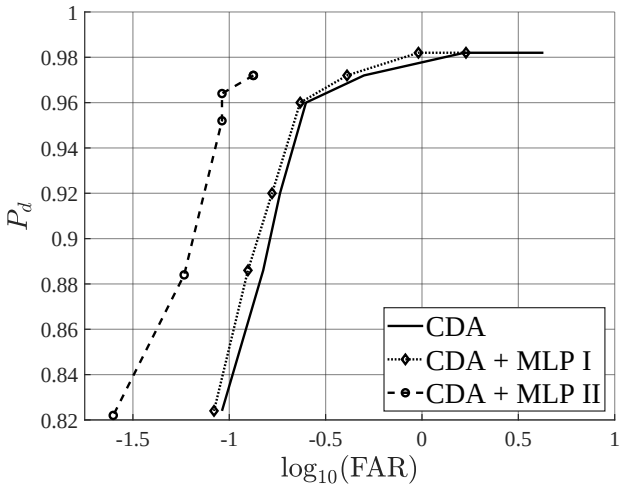

Fig. 8. Comparison between CDA performance and systems with the discriminator algorithm.

Both Figure 8 and Table I demonstrate a large difference in performance between the CDA and its use in combination with the discriminator algorithm. Performance improvement is noticeable when the network is trained with samples of false alarms previously detected (e.g., fences and power lines). This is due to the fact that the approach used to train the MLP II considers a more realistic case of target discrimination, which although achieving a theoretical precision lower than the MLP I, ends up being more suitable to the problem.

V. Conclusions

In this paper, a system compounded of a CDA and a discriminator algorithm is proposed in order to re-evaluate the detections initially pointed out by the first one. The results indicated a performance improvement by reducing false alarms with an extremely low computational cost, since the MLP model can be pre-trained. The false alarm reduction achieved indicates that a CDA which favors a high probability of detection (even with a high false alarm rate) can be preferable to the application, as the discriminator algorithm can compensate these flaws. This can cause a simplification of the threshold establishment process, as the main concern of a change detection algorithm is to maintain a low FAR. By dismembering the problem of target detection into two algorithms, a greater permissiveness of the CDA is allowed, i.e., to use the first algorithm to maximize target detection and ensure a high P_d, leaving to the MLP the task of eliminating (or reducing) false alarms. Future works can address the computational complexity of the proposed model in comparison to known costly algorithms approaches, such as ones that use techniques like constant false alarm rate (CFAR) filters and likelihood ratio tests (e.g., [20], [21]).

Acknowledgements

The authors would like to thank: the Swedish Defence Research Agency (FOI) and SAAB AB for providing the CARABAS-II SAR data; the Brazilian National Council for Scientific and Technological Development (CNPq) and the Coordination for the Improvement of Higher Education Personnel (CAPES) for the financial support.

References

[1] A. Moreira, P. Prats-Iraola, M. Younis, G. Krieger, I. Hajnsek, and K. P. Papathanassiou, "A tutorial on synthetic aperture radar," *IEEE Geoscience and remote sensing magazine*, vol. 1, no. 1, pp. 6–43, 2013.

[2] T. Zhou, J. Pan, P. Zhang, S. Wei, and T. Han, "Mapping winter wheat with multi-temporal sar and optical images in an urban agricultural region," *Sensors (Basel)*, vol. 17, no. 6, p. 1210, 2017.

[3] J. Reiche, C. M. Souza, D. K. Hoekman, J. Verbesselt, and H. Persaud, "Feature level fusion of multi-temporal alos palsar and landsat data for mapping and monitoring of tropical deforestation and forest degradation," *IEEE Journal of Selected Topics in Applied Earth Observations and Remote Sensing*, vol. 6, pp. 2159 – 2173, 2013.

[4] Y. Ban and O. A. Yousif, "Multitemporal spaceborne sar data for urban change detection in china," *IEEE Journal of Selected Topics in Applied Earth Observations and Remote Sensing*, vol. 5, pp. 1087 – 1094, 2012.

[5] J. Hugenschmidt and R. Loser, "Detection of chlorides and moisture in concrete structures with ground penetrating radar," *Materials and Structures*, vol. 41, no. 4, pp. 785–792, 2008.

[6] L. M. H. Ulander, P. O. Frölind, A. Gustavsson, H. Hellsten, and B. Larsson, "Detection of concealed ground targets in CARABAS SAR imagens using change detection," *Proceedings of SPIE*, pp. 243–252, 1999.

[7] M. Lundberg, L. M. H. Ulander, W. E. Pierson, and A. Gustavsson, "A challenge problem for detection of targets in foliage," *Proceedings of SPIE*, 2006.

[8] J. Facon, "A morfologia matemática e suas aplicações em processamento de imagens," in *VII Workshop de Visão Computacional–WVC*, vol. 13, 2011.

[9] R. D. Molin Jr, A. C. F. Fabrin, P. Sperotto, D. I. Alves, F. M. Bayer, R. Machado, M. I. Pettersson, H. Hellsten, P. Dammert, and L. Ulander, "Iterative change detection algorithm for low-frequency uwb sar," in *XXXIV Simpósio Brasileiro de Telecomunicações e Processamento de Sinais (SBrT 2016), Santarém, Brasil*, 2016, pp. 654–658.

[10] D. C. Montgomery, *Introduction to Statistical Quality Control*, 6th ed. John Wiley & Sons, Inc., 2009, no. 4.

[11] L. P. Ramos, V. I. A. Medeiros, D. I. Alves, C. Muller, R. Machado, and B. F. Uchoa-Filho, "Influência de operações morfológicas em algoritmo de detecção de alvos para imagens sar vhf uwb," in *XXXVII Simpósio Brasileiro de Telecomunicações e Processamento de Sinais (SBrT 2018), Campina Grande, Brasil*, 2018, pp. 747–751.

[12] L. V. Fausett *et al.*, *Fundamentals of neural networks: architectures, algorithms, and applications*. prentice-Hall Englewood Cliffs, 1994, vol. 3.

[13] M. T. Hagan, H. B. Demuth, M. H. Beale, and O. De Jesús, *Neural network design*. Pws Pub. Boston, 1996, vol. 20.

[14] Q. Zhao and J. C. Principe, "Support vector machines for sar automatic target recognition," *IEEE Transactions on Aerospace and Electronic Systems*, vol. 37, no. 2, pp. 643–654, 2001.

[15] N. M. Sandirasegaram, "Automatic target recognition in sar imagery using a mlp neural network," Defence Research and Development Canada Ottawa, Tech. Rep., 2002.

[16] X. Tang, L. Zhang, and X. Ding, "Sar image despeckling with a multilayer perceptron neural network," *International Journal of Digital Earth*, vol. 12, no. 3, pp. 354–374, 2019.

[17] S. Haykin, *Neural networks and learning machines*. Pearson education Upper Saddle River, 2009, vol. 3.

[18] W. Ye, C. Paulson, D. O. Wu, and J. Li, "A target detection scheme for vhf sar ground surveillance," in *Algorithms for Synthetic Aperture Radar Imagery XV*, vol. 6970. International Society for Optics and Photonics, 2008, p. 69700Y.

[19] C. E. Metz, "Basic principles of ROC analysis," *Seminars in Nuclear Medicine*, vol. 8, no. 4, pp. 283–298, 1978.

[20] L. Ulander, M. Lundberg, W. Pierson, and A. Gustavsson, "Change detection for low-frequency SAR ground surveillance," *IEE Proceedings - Radar, Sonar and Navigation*, vol. 152, no. 6, pp. 413–420, 2005.

[21] N. R. Gomes, P. Dammert, M. I. Pettersson, V. T. Vu, and H. Hellsten, "Comparison of the rayleigh and k-distributions for application in incoherent change detection," *IEEE Geoscience and Remote Sensing Letters*, 2018.